

Article

Methanol Steam Reforming over $\text{La}_{1-x}\text{Sr}_x\text{CeO}_{3-\delta}$ Catalysts for Hydrogen Production: Optimization of Operating Parameters

Gaokui Chen, Qiuwan Shen ^{*}, Xin Zhang, Zhongwen Cai, Zicheng Shao, Shian Li  and Guogang Yang 

Marine Engineering College, Dalian Maritime University, Dalian 116026, China

^{*} Correspondence: shenqiuwan@dlnu.edu.cn

Abstract: In this study, a series of A-site strontium-doped $\text{La}_{1-x}\text{Sr}_x\text{CeO}_{3-\delta}$ ($x = 0.2, 0.4, 0.6, 0.8$) perovskite catalysts were synthesized via the ethylenediaminetetraacetic acid (EDTA) sol-gel method for hydrogen production by methanol steam reforming. The fresh and the reduced catalysts are characterized by scanning X-ray (XRD), energy dispersive X-ray spectroscopy (EDS) and scanning electron microscopy (SEM) techniques. Results showed that $\text{La}_{0.6}\text{Sr}_{0.4}\text{CeO}_{3-\delta}$ exhibited the best performance among the $\text{La}_{1-x}\text{Sr}_x\text{CeO}_{3-\delta}$ catalysts. The operating parameters were optimized to study the catalytic performance of $\text{La}_{0.6}\text{Sr}_{0.4}\text{CeO}_{3-\delta}$, including catalytic temperature, water–methanol ratio (W/M) and liquid hourly space velocity (LHSV). However, the excessive strontium content led to a decrease in hydrogen production amount per unit time, and the high W/M promoted the reverse water–gas shift reaction (RWGS), which resulted in a decrease in CO selectivity and an increase in CO_2 selectivity. In addition, the optimal reaction parameters are as follows: reforming temperature of 700 °C; W/M of 3:1; LHSV of 20 h^{-1} . Furthermore, the methanol conversion rate of $\text{La}_{0.6}\text{Sr}_{0.4}\text{CeO}_{3-\delta}$ can reach approximately 82%, the hydrogen production can reach approximately $3.26 \times 10^{-3} \text{ mol/g}_{(\text{cat})}/\text{min}$ under the optimum reaction conditions. Furthermore, $\text{La}_{0.6}\text{Sr}_{0.4}\text{CeO}_{3-\delta}$ exhibits high hydrogen selectivity (85%), which is a promising catalyst for MSR application.

Keywords: $\text{La}_{0.6}\text{Sr}_{0.4}\text{CeO}_{3-\delta}$; methanol steam reforming; Sr doping; optimal operation parameters

Citation: Chen, G.; Shen, Q.; Zhang, X.; Cai, Z.; Shao, Z.; Li, S.; Yang, G. Methanol Steam Reforming over $\text{La}_{1-x}\text{Sr}_x\text{CeO}_{3-\delta}$ Catalysts for Hydrogen Production: Optimization of Operating Parameters. *Catalysts* **2023**, *13*, 248. <https://doi.org/10.3390/catal13020248>

Academic Editor: Leonarda Liotta

Received: 26 December 2022

Revised: 14 January 2023

Accepted: 19 January 2023

Published: 21 January 2023



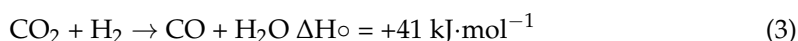
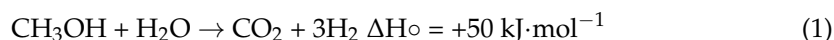
Copyright: © 2023 by the authors. Licensee MDPI, Basel, Switzerland. This article is an open access article distributed under the terms and conditions of the Creative Commons Attribution (CC BY) license (<https://creativecommons.org/licenses/by/4.0/>).

1. Introduction

Hydrogen is considered an efficient and clean energy that is a promising alternative energy to fossil fuels. Hydrogen combustion can generate higher energy density, along with water, and will not produce greenhouse gases such as carbon dioxide, rendering it a form of clean energy [1]. Meanwhile, hydrogen is considered the key pathway for deep decarbonization in the energy and transportation sectors, which is widely utilized in the chemical and petroleum industries. It was also identified as one of the most promising clean energy sources for power generation and fuel cell equipment [2].

Although hydrogen shows great potential as an alternative energy source, it still faces many challenges, such as storage and transportation of hydrogen being major limitations and the need for high pressure and low temperature conditions for hydrogen storage systems compared to conventional fuels, which will make production more expensive and dangerous [3]. In order to overcome these challenges, researchers have combined renewable energy with hydrogen energy and conducted much research on new fuels that can provide hydrogen-rich gas for fuel cells. At present, liquid fuel as a hydrogen carrier is a promising way to produce on-line hydrogen for vehicles or other devices [4]. Among them, methanol has received extensive attention. At room temperature, methanol is a liquid without C-C bonds that is easy to store and transport. It has high H/C ratio, high hydrogen content, high energy density and high hydrogen yield, and the methanol hydrogen production device is relatively simple. In addition, methanol is also a carbon neutral renewable raw material, and its production is also economically sustainable, as it can be prepared from fossil resources as well as biomass. Methanol dry reforming (DR) [5],

methanol steam reforming (MSR) [6], methanol partial oxidation (POX) [7], and methanol self-thermal reforming (ATR) [8] are currently the four main methods utilized to transform methanol into hydrogen-rich gas. When compared to the other technologies, MSR has some advantages due to its low CO yield and high H/C ratio [9]. Furthermore, the MSR process involves a simpler catalytic reaction and easier temperature control. The MSR reaction can be represented by (Equation (1)). However, there are two common side reactions in the MSR reaction, the direct methanol decomposition reaction (Equation (2)) and the water–gas conversion inverse reaction (Equation (3)). Special attention should be paid to the concentration of CO in the reaction, as CO can be hazardous to the electrical electrodes of the fuel cell.



The reaction performance of MSR mainly depends on the catalyst, thus, an ideal catalyst could avoid side reactions, prevent deactivation caused by carbon deposition, and improve the selectivity of hydrogen. Due to their distinctive crystal structure and catalytic properties, perovskite oxides (ABO_3) have attracted a lot of attention. A-site is an alkaline earth or rare earth element, while B-site is typically a transition element. Both A- and B-sites can be partially replaced by metal ions, which will change their catalytic, structural and redox properties, thus, improving catalytic activity and stability.

Wu et al. [10] synthesized $\text{La}_{1-x}\text{Ca}_x\text{NiO}_3$ perovskite-type oxides. The results indicated that the doping of Ca at A-site resulted in a strong metal–carrier interaction and produced a high metal dispersion, which inhibited the deposition of carbon and improved the stability of the catalyst. Zhang et al. [11] synthesized $\text{LaNiO}_{3-\delta}$ nanoparticles that were undoped and doped with strontium by the sol-gel method. The results indicated that strontium doping can introduce more oxygen vacancies in $\text{LaNiO}_{3-\delta}$, and catalytic performance than undoped $\text{LaNiO}_{3-\delta}$. Morales et al. [12] prepared $\text{La}_{0.6}\text{Sr}_{0.4}\text{CoO}_{3-\delta}$ perovskite catalysts, and they discovered that a tiny quantity of Sr can make the cobalt nanoparticles extensively dispersed on a carrier composed of metal carbonates and metal oxides and boost the catalytic activity. Additionally, the presence of strontium oxide decreases the production of CO. Ma et al. [13] prepared an LaXCoO_3 ($X = \text{Mg}, \text{Ca}, \text{Sr}, \text{Ce}$) perovskite composite catalyst by the citric acid complex method for hydrogen production from ethanol steam. The results showed that Sr-doped samples exhibited excellent activity and stability and showed better catalytic performance than the other samples. Cui et al. [14] pointed out that the catalyst containing Ce has high hydrogen storage capacity, can effectively disperse active metals and inhibit sintering, and Ce can also promote the gasification of carbon substances. The B-site element of perovskite plays an important role in its catalytic performance. Gómez et al. [15] synthesized an $\text{La}_{0.8}\text{Sr}_{0.2}\text{Fe}_{0.8}\text{Cr}_{0.2}\text{O}_3$ perovskite oxide using a polymerization chemical route, and they demonstrated that $\text{La}_{0.8}\text{Sr}_{0.2}\text{Fe}_{0.8}\text{Cr}_{0.2}\text{O}_3$ had higher stability and a lower deactivation rate than LaFeO_3 , as well as better selectivity for hydrogen and methane conversion up to 95%. It demonstrates that the catalyst with the added promoter has better catalytic activity. Natile et al. [16] studied the influence of Co/Fe elements on the physicochemical properties of $\text{La}_{0.6}\text{Sr}_{0.4}\text{Co}_{1-y}\text{Fe}_y\text{O}_{3-\delta}$ ($y = 0.2, 0.5, 0.8$) as a methanol/ethanol steam reforming catalyst. They found that the iron element at the B-site can inhibit the formation of by-product CO, especially when the CO/Fe molar ratio is greater than 1. Shen's research group [17,18] prepared perovskite oxides with different amounts of Co doping by the sol-gel method. The results showed that the doping amount of cobalt at B-site could affect the selectivity of gas phase products through the balance of the water–gas transfer reaction, and the effect of Al_2O_3 support derived from metal-organic framework on the performance of $\text{LaNi}_{0.4}\text{Al}_{0.6}\text{O}_{3-\delta}$ for MSR was studied. The results show that the interaction between the carrier and the active component is strengthened, the dispersion of the active component is improved, the methanol conversion is increased, and the thermal stability is excellent.

Although some studies were conducted on the MSR performance of Lanthanide perovskite, there are few reports using La-Ce-based perovskites as catalysts for MSR. The purpose of this paper is to develop a La-Ce-based perovskite catalyst with high catalytic activity and selectivity for H₂ production. Furthermore, the Sr-doping effects, optimal operating conditions for the hydrogen production performance of the synthesized perovskites were investigated in the MSR, which can provide a support for the practical development of the hydrogen energy economy.

2. Results and Discussion

2.1. XRD, SEM and SEM-EDS

The fresh and hydrogen-reduced perovskite La_{0.6}Sr_{0.4}CeO_{3-δ} were examined by XRD to identify the crystalline phase, as shown in Figure 1. It can be seen from the figure that the strong diffraction peak of fresh La_{0.6}Sr_{0.4}CeO_{3-δ} shows the characteristics of the typical perovskite structure as reported in the literature [19], which demonstrates that the lanthanide perovskite-type oxides were successfully synthesized. Generally, the catalysts applied to methanol steam reforming are subjected to pre-reduction treatment. Therefore, the comparison of XRD patterns of La_{0.6}Sr_{0.4}CeO_{3-δ} catalysts before and after reduction by hydrogen can also be seen in Figure 1. The results indicated that the catalyst still maintains the original structure after hydrogen reduction treatment and exhibits a very typical perovskite structure because La_{0.6}Sr_{0.4}CeO_{3-δ} perovskite metal oxides are difficult to reduce with hydrogen. The result is consistent with Shen's study [18]. The reason for this phenomenon may be that the La_{0.6}Sr_{0.4}CeO_{3-δ} catalyst is a cubic structure [20] and exhibits diffraction corresponding to the cubic perovskite structure ($2\theta = 32.7^\circ, 37.9^\circ$ and 54.5°), and some studies have confirmed that the cubic perovskite structure is stable in a reducing environment [21].

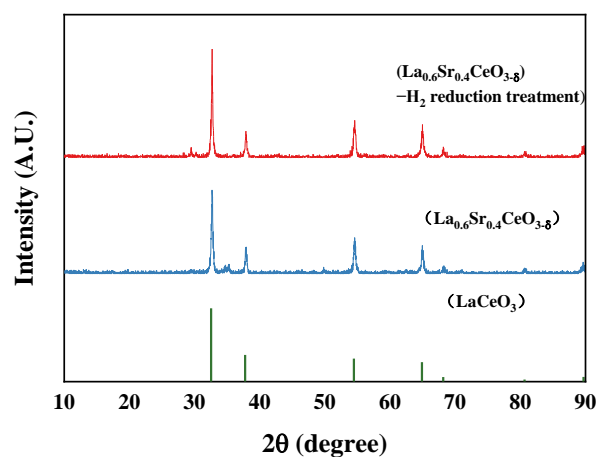


Figure 1. XRD pattern of La_{0.6}Sr_{0.4}CeO_{3-δ} catalysts before and after reduction by hydrogen.

In order to more intuitively comprehend the difference in surface morphology between the fresh La_{0.6}Sr_{0.4}CeO_{3-δ} and the reduced La_{0.6}Sr_{0.4}CeO_{3-δ}, the SEM characterization of the two catalysts was carried out, as shown in Figure 2. It can be seen from Figure 2a that the particle size is not uniform, and there were some lumpy particles in the fresh La_{0.6}Sr_{0.4}CeO_{3-δ} sample, showing the characteristics of aggregation. Figure 2b shows the SEM images of La_{0.6}Sr_{0.4}CeO_{3-δ} powders reduced by H₂. Compared with the fresh samples, the surface morphological characteristics of the La_{0.6}Sr_{0.4}CeO_{3-δ} catalyst samples after the hydrogen reduction treatment did not change significantly. However, there was a partial reduction in the massive particles, and a certain number of small independent particles appeared that had a more uniform particle distribution and roughly the same particle size, so the activity of the reduced treated catalyst was excellent [22,23].

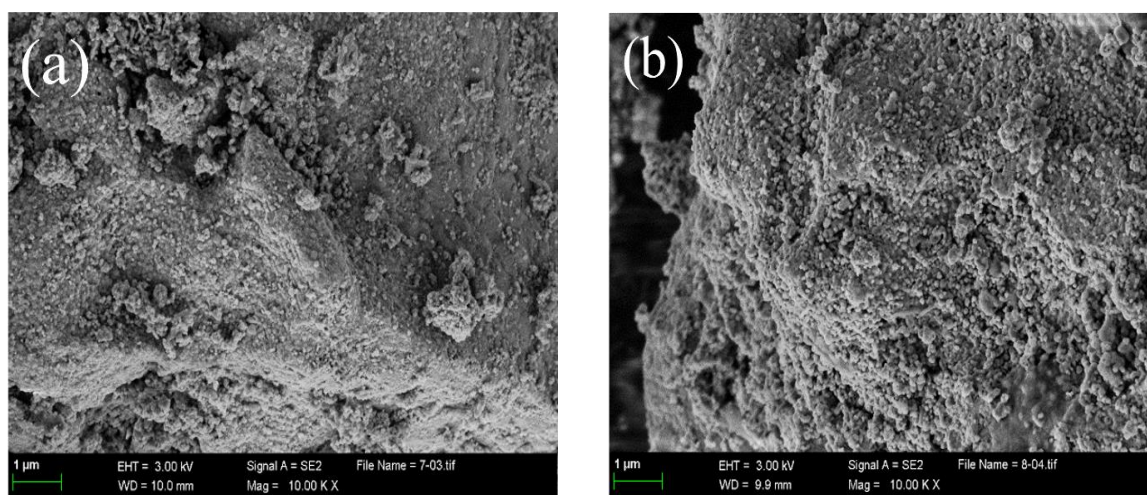


Figure 2. SEM images of (a) the fresh $\text{La}_{0.6}\text{Sr}_{0.4}\text{CeO}_{3-\delta}$ sample, (b) the $\text{La}_{0.6}\text{Sr}_{0.4}\text{CeO}_{3-\delta}$ sample after reduction treatment.

Energy dispersive X-ray spectroscopy (EDS) was used to analyze the element composition (Figure 3). The correct elemental composition was observed for all characterized samples, and all the elements were uniformly distributed on the catalyst particles. Figure 3a shows the selected area of SEM-EDS mapping, The composition and distribution of each element in the synthesized catalyst material are shown in Figure 3b–e, and all elements are: La, Sr, Ce and O. In addition, the elemental composition of the synthesized catalyst was determined by SEM-EDS. The atomic ratio and nominal atoms of the main elements before and after sample reduction are shown in Table 1. The element ratio of the prepared catalyst sample and the standard element ratio are within the allowable error range, considering the accuracy of SEM-EDS characterization. Therefore, combining the results of EDS and XRD, it can be determined that the perovskite metal oxide catalyst was successfully synthesized. In addition, it can also be seen that the element ratio and standard element ratio of the catalyst sample after reduction are also within the allowable error range, indicating that the perovskite structure has not changed, which is consistent with the XRD results.

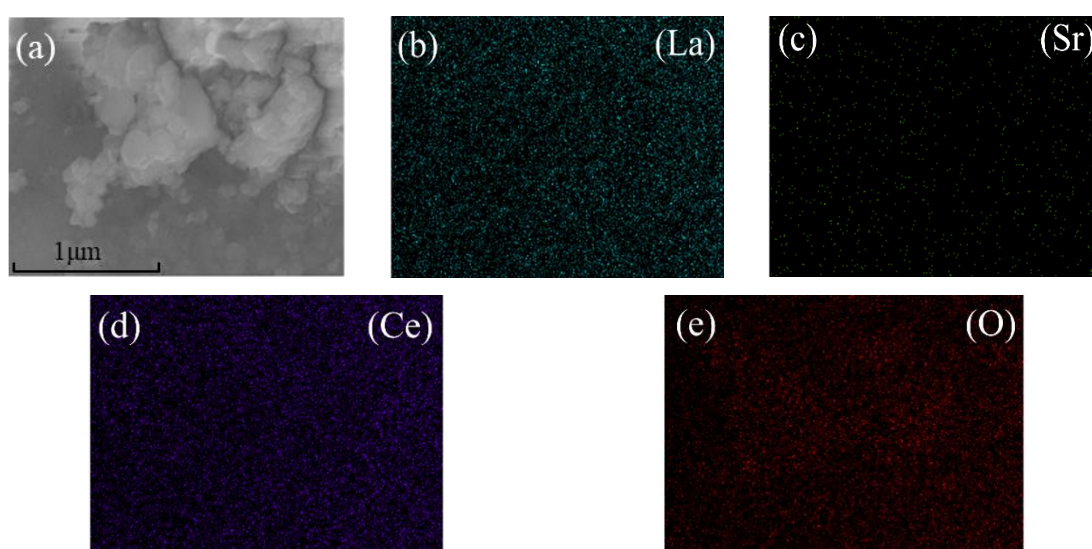


Figure 3. SEM-EDS mapping images of the fresh $\text{La}_{0.6}\text{Sr}_{0.4}\text{CeO}_{3-\delta}$: (a) the selected area of SEM-EDS mapping; (b) lanthanum; (c) strontium; (d) cerium; (e) oxygen.

Table 1. The SEM-EDS data of the $\text{La}_{0.6}\text{Sr}_{0.4}\text{CeO}_{3-\delta}$ sample.

Elements	Standard Atomic Ratio	Atomic Ratio of the Fresh $\text{La}_{0.6}\text{Sr}_{0.4}\text{CeO}_{3-\delta}$	Atomic Ratio of the $\text{La}_{0.6}\text{Sr}_{0.4}\text{CeO}_{3-\delta}$ Reduced by H_2
La	9	8.76	3.64
Sr	6	5.87	1.82
Ce	15	15.10	6.33

2.2. Catalytic Performance

2.2.1. The Effects of A-Site Doping

The composition and ratios of the A/B-site elements of perovskite metal oxides have a great influence on its catalytic activity [24]. The ions on the A-site indirectly promote the catalytic activity. When the A-site ions are replaced, more defects are produced, which affects the electronic state of the B-site ions [25]. A- and B-sites play different roles in the reaction process. B-site mainly affects the temperature range of the reaction, and A-site mainly affects the selectivity of the reaction [26]. In general, Sr was partially substituted for La-site in the perovskite structure to improve the lattice oxygen mobility, which plays a role in the reforming reaction and coke removal [27]. The effect of Sr doping on the catalytic performance of $\text{La}_{1-x}\text{Sr}_x\text{CeO}_{3-\delta}$ ($x = 0.2, 0.4, 0.6, 0.8$) in MSR was investigated in this study. The MSR performance test results of the catalyst are shown in Figure 4 (the reaction temperature is $600\text{ }^\circ\text{C}$; the molar ratio of water to methanol (W/M) is 3:1; the liquid hourly space velocity (LHSV) is 20 h^{-1}).

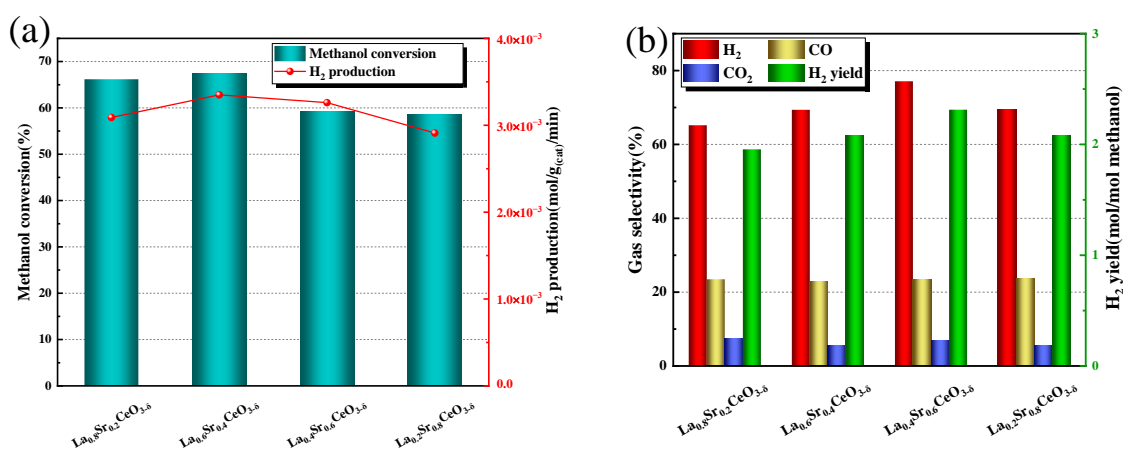


Figure 4. The MSR catalytic performance of the $\text{La}_{1-x}\text{Sr}_x\text{CeO}_{3-\delta}$ ($x = 0.2, 0.4, 0.6, 0.8$): (a) methanol conversion (left Y) and hydrogen production of 1g catalyst (right Y); (b) gas selectivity (left Y) and hydrogen yield (right Y).

As shown in Figure 4a, with the increase in A-site strontium doping amount in perovskite, the methanol conversion first increased and then decreased, among which the strontium doping amount was 0.2 and 0.4, the methanol conversion had no change (approximately 68%); however, when the strontium doping amount was increased to 0.6 or 0.8, the methanol conversion was reduced to 60%. In addition, it was obvious from Figure 4a that strontium doping also showed some influence on hydrogen production. Similar to methanol conversion, hydrogen production displayed a trend of first increasing and then decreasing. $\text{La}_{0.6}\text{Sr}_{0.4}\text{CeO}_{3-\delta}$ exhibited the best performance and the maximum hydrogen production per unit time was $3.5 \times 10^{-3}\text{ mol/g}_{(\text{cat})}/\text{min}$. As shown in Figure 4b, with the addition of strontium, the gas selectivity of carbon dioxide and carbon monoxide was basically unchanged, indicating that the concentration of strontium at position A had no significant effect on the selectivity of by-products. However, excessive strontium content led to a decrease in H_2 selectivity and H_2 yield.

In conclusion, considering that methanol conversion and hydrogen production per unit time can best reflect the performance of a methanol steam reforming catalyst, $\text{La}_{0.6}\text{Sr}_{0.4}\text{CeO}_{3-\delta}$ exhibited the highest methanol conversion and hydrogen production per unit time, and therefore, it was selected as a candidate for subsequent experiments. Generally, the catalytic performance was also affected by the experimental operating conditions. Therefore, the effects of reforming temperature, W/M and LHSV on MSR were studied.

2.2.2. The Effects of Reforming Temperature

MSR is a strongly endothermic reaction [28], so its catalytic performance is most affected by the reforming temperature. Figure 5 shows the MSR performance of the $\text{La}_{0.6}\text{Sr}_{0.4}\text{CeO}_{3-\delta}$ at different reforming temperatures. From Figure 5a, it can be concluded that temperature has a significant effect on methanol conversion and hydrogen production. When the reforming temperature was 500 °C, the methanol conversion and hydrogen production were significantly different from other temperatures. The methanol conversion was less than 10%, and the hydrogen production per unit time was only $0.3 \times 10^{-3} \text{ mol/g}_{(\text{cat})}/\text{min}$, probably because MSR is a strong heat-absorbing reaction and low temperature cannot provide enough energy [29]. With the increase in reforming temperature, the methanol conversion (73%) and hydrogen production ($3.78 \times 10^{-3} \text{ mol/g}_{(\text{cat})}/\text{min}$) reached the maximum at 700 °C. However, when the temperature rises to 800 °C, methanol conversion and hydrogen production per unit time will decrease. The reason was catalyst sintering caused by high temperatures [30]. As shown in Figure 5b, both hydrogen selectivity and hydrogen yield decrease first and then increase with the increase in reforming temperature. However, the selectivity of CO increases first and then decreases. This may be because the methanol decomposition reaction (Equation (2)) requires more energy than the MSR reaction (Equation (1)), so methanol decomposition reaction was inhibited at a low temperature. When the temperature continued to rise, the reverse process of water–gas shift reaction was promoted, thus, increasing the selectivity of CO_2 . In general, the temperature with the highest methanol conversion and hydrogen production per unit time, 700 °C, was identified as the optimal reforming temperature.

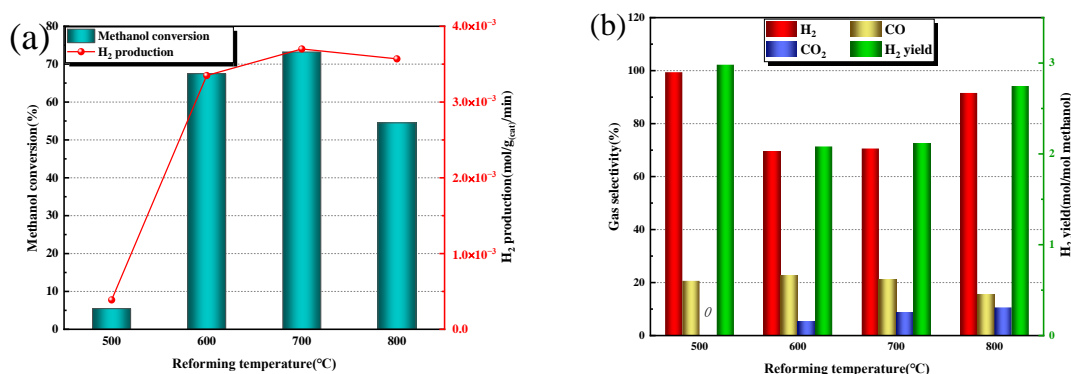


Figure 5. The MSR performance of the $\text{La}_{0.6}\text{Sr}_{0.4}\text{CeO}_{3-\delta}$ at different reforming temperatures: (a) methanol conversion (left Y) and hydrogen production of 1 g catalyst (right Y); (b) gas selectivity (left Y) and hydrogen yield (right Y).

2.2.3. The Effects of the W/M

The hydrogen element in the MSR reaction is partly from water and partly from methanol [31], and the presence of water vapor has a certain impact on the water–gas shift reaction. Therefore, the W/M is also one of the factors affecting the catalytic performance of MSR. In this section, four experiments concerning methanol steam reforming were carried out with the W/M as the research object (the reforming temperature is 700 °C; the LHSV is 20 h^{-1}). The influence of different W/M on catalytic performance is shown in

Figure 6. As shown in Figure 6a, when the molar ratio of water to methanol was 2:1, 4:1, 5:1, there was no significant difference in methanol conversion, but when W/M was 3:1, methanol conversion reached the maximum value, and hydrogen production showed a decreasing trend. In addition, a smaller W/M meant that more methanol was needed, and the methanol conversion decreased at the same time, which leads to waste of methanol and increased cost. Figure 6b indicates that the high W/M can suppress the CO selectivity, which may be related to the water–gas shift reaction. The high W/M promoted the reverse process of the WGSR reaction, as shown in Equation (3). However, considering that methanol conversion and hydrogen production can best reflect the catalyst performance of methanol steam reforming, the best water-to-methanol molar ratio for the next experiment was determined to be W/M of 3:1.

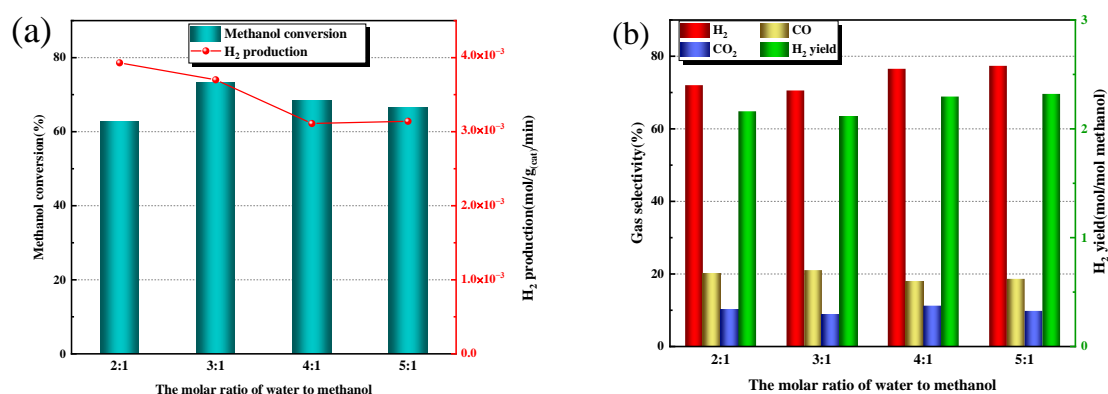


Figure 6. The MSR performance of the $\text{La}_{0.6}\text{Sr}_{0.4}\text{CeO}_{3-\delta}$ at different W/M: (a) methanol conversion (left Y) and hydrogen production of 1g catalyst (right Y); (b) gas selectivity (left Y) and hydrogen yield (right Y).

2.2.4. The Effects of the LHSV

The liquid hourly space velocity (LHSV) was also one of the factors affecting the performance of methanol steam reforming. The liquid refers to methanol and water. In order to explore the influence of LHSV on the performance of reforming reaction, MSR experiments were carried out at 10 h^{-1} , 15 h^{-1} , 20 h^{-1} and 25 h^{-1} , respectively, (reforming temperature is $700\text{ }^{\circ}\text{C}$; W/M is 3:1). The experimental results were shown in Figure 7. The influence of different LHSV on the catalytic activity of the catalyst and the selectivity/yield of gas products are shown in Figure 7a,b, respectively. It can be seen from Figure 7a that methanol conversion reaches the maximum value of 82% at LHSV of 20 h^{-1} , while hydrogen production increases with the increase in LHSV. However, LHSV should not be too high, because too high airspeed will lead to a decline in the methanol conversion rate, resulting in waste of methanol. It can be seen from Figure 7b that the LHSV has small influence on the selectivity of gas products and the yield of hydrogen. Furthermore, the trend of hydrogen selectivity was similar to that of hydrogen yield, both of which were decreasing first and then increasing. In addition, the selectivity of CO decreased first and then increased, while the selectivity of CO₂ exhibits the opposite trend. In summary, the reforming temperature of $700\text{ }^{\circ}\text{C}$, the W/M of 3:1 and the LHSV of 20 h^{-1} were the optimal experimental conditions for perovskite oxide $\text{La}_{0.6}\text{Sr}_{0.4}\text{CeO}_{3-\delta}$ in MSR.

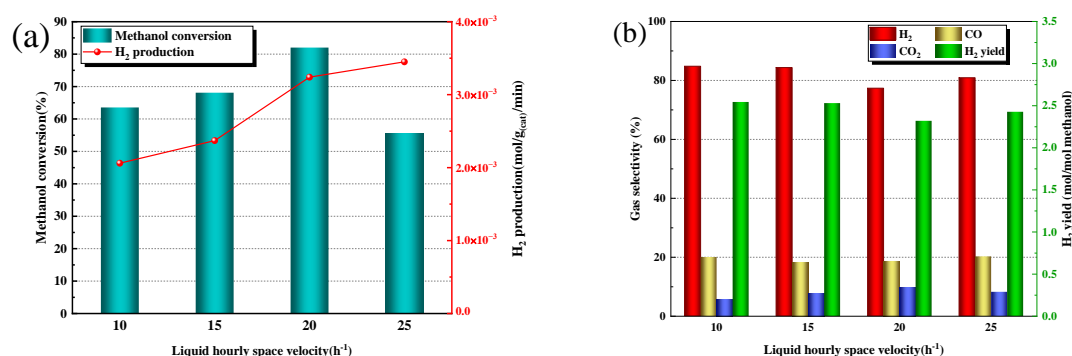


Figure 7. The MSR performance of the $\text{La}_{0.6}\text{Sr}_{0.4}\text{CeO}_{3-\delta}$ at different LHSV: (a) methanol conversion (left Y) and hydrogen production of 1 g catalyst (right Y); (b) gas selectivity (left Y) and hydrogen yield (right Y).

3. Materials and Methods

3.1. Preparation of $\text{La}_{1-x}\text{Sr}_x\text{CeO}_{3-\delta}$ Perovskite Powders

The perovskite-type metal oxide catalyst was prepared by the sol-gel method with citric acid as a complexing agent and ethylenediaminetetraacetic EDTA acid as an auxiliary complexing agent. $\text{La}(\text{NO}_3)_3 \cdot 6\text{H}_2\text{O}$ (99%), $\text{Sr}(\text{NO}_3)_2$ (99%) and $\text{Ce}(\text{NO}_3)_2 \cdot 6\text{H}_2\text{O}$ (99%) were applied as the raw materials for metal precursors, which were obtained from the Aladdin Corporation. For preparing 0.02 mol perovskite powder as an example, first, the required metal precursors were weighed, added to approximately 120 mL of deionized water and stirred to dissolve. Then, the precursor solution was supplemented with a certain proportion of citric acid and ethylenediaminetetraacetic acid while being stirred, and the molar ratio of metal nitrate, citric acid and EDTA was 1:1.5:1 [32]. The resulting mixture was stirred in a water bath at 80 °C for 4–5 h to obtain the gel. The gel was then dried for 12 h at 110 °C in a drying oven to obtain a fluffy structured substance. The resulting fluffy substance was milled into a powder and put in a muffle furnace to calcine for 30 min at 400 °C and then for 7 h at 850 °C. The purpose of calcination was to remove organic compounds [33]. Finally, the calcined material was ground to obtain the final perovskite catalyst.

3.2. Characterization

The samples were characterized by X-ray diffraction (D/MAX-Ultima+ diffractometer), and the phase composition of the samples was determined with a $\text{Co-K}\alpha$ monochromatic X-ray source (1.7902 Å, 40 kV, 40 mA). The diffraction patterns in the range of 2θ of 10–90° were recorded with a scanning step of 0.02°. The surface morphology (SEM) and chemical composition (EDS) of the synthesized samples was analyzed by scanning electron microscopy (SUPRA 55 SAPPHIRE, ZEISS, Jena, Germany).

3.3. Methanol Steam Reforming Experiments

The synthesized perovskite catalyst sample was used in the MSR reaction for hydrogen production. First, 0.3 g of catalyst was weighed and placed into the middle of a quartz tube, where the reaction temperature was controlled by a thermocouple in the tube furnace. The mass flow controller was responsible for regulating the gas flow rate in the MSR experiment.

The temperature of the reactor was first heated from room temperature to 300 °C while being purged with 30 mL/min of nitrogen. The temperature was then raised to 600 °C and the catalyst sample was reduced under a mixture gas of 10% H_2 –90% N_2 for 40 min. Following this, the experimental system was purged with N_2 at a catalytic temperature. The configured mixed solution of water and methanol was mounted on a micro-pump and pumped to the steam generator at 130 °C according to the preset feed flow rate, where it turned into steam, and subsequently, the methanol water vapor was brought into the reactor at 30 mL/min N_2 . The volume concentrations of H_2 , CO and CO_2 were recorded

with an on-line gas analyzer, and methanol conversion, the H₂ yield, the selectivity of gas products and hydrogen production per unit time were calculated as follows:

$$X_{\text{methanol}} = \left(1 - \frac{n_{\text{methanol}}^{\text{out}}}{n_{\text{methanol}}^{\text{in}}}\right) \times 100\% \quad (4)$$

$$Y_{\text{H}_2} = \frac{F_{\text{H}_2}}{n_{\text{methanol}}^{\text{in}}} \quad (5)$$

$$S_{\text{H}_2} = \frac{F_{\text{H}_2}}{(n_{\text{methanol}}^{\text{in}} - n_{\text{methanol}}^{\text{out}}) \times 3} \times 100\% \quad (6)$$

$$S_i = \frac{F_i}{F_{\text{CO}} + F_{\text{CO}_2} + F_{\text{H}_2}} \times 100\% \quad (7)$$

$$P_{\text{H}_2} = \frac{C_{\text{H}_2} \times f_{\text{products}}}{m_{\text{cat}} \times 10^6} \quad (8)$$

where X_{methanol} (%), Y_{H_2} (mol/mol methanol), S_{H_2} (%), S_i (%), $i = \text{CO}, \text{CO}_2$) and P_{H_2} (mol/g_(cat)/min) were the CH₃OH conversion, H₂ yield, H₂ selectivity, the CO/CO₂ selectivity and hydrogen production of 1 g catalyst, respectively. More information on the parameter annotations in the equations was provided in the previous literature [17].

4. Conclusions

La_{1-x}Sr_xCeO_{3-δ} ($x = 0.2, 0.4, 0.6, 0.8$) perovskite powders were synthesized by the sol-gel method and applied for MSR to produce H₂. The effect of Sr doping and the reaction conditions of La_{0.6}Sr_{0.4}CeO_{3-δ} perovskite powders were studied in-depth by characterization with SEM, XRD, EDS and the MSR experiments. The main conclusions are as follows:

1. The experimental results showed that La_{0.6}Sr_{0.4}CeO_{3-δ} has the highest methanol conversion and hydrogen production per unit time among the La_{1-x}Sr_xCeO_{3-δ}. In addition, excessive Sr content led to a decrease in H₂ selectivity and H₂ yield.
2. The results of XRD and SEM-EDS showed that the La_{0.6}Sr_{0.4}CeO_{3-δ} catalyst was successfully synthesized in this study. The catalyst still maintains the original structure after hydrogen reduction treatment and exhibits a very typical perovskite structure because La_{0.6}Sr_{0.4}CeO_{3-δ} perovskite metal oxides are difficult to reduce with hydrogen. The reason for this phenomenon may be that the La_{0.6}Sr_{0.4}CeO_{3-δ} catalyst is a cubic structure, and some studies have confirmed that the cubic perovskite structure is stable in a reducing environment. The results of SEM indicated that the surface morphology of the catalyst sample after reduction treatment did not change significantly compared with that of the fresh sample. The reduced catalyst sample has more uniform particle distribution and roughly the same particle size, so the catalyst activity is more excellent.
3. The influence of experimental conditions on the catalytic performance of La_{0.6}Sr_{0.4}CeO_{3-δ} catalyst was investigated in this study, and the optimal reforming temperature, W/M and LHSV were determined to be 700 °C, 3:1 and 20 h⁻¹, respectively. The maximum methanol conversion rate was 82%, and the hydrogen production per unit time could reach 3.2×10^{-3} mol/g_(cat)/min. La_{0.6}Sr_{0.4}CeO_{3-δ} is a potential catalyst for methanol steam reforming with good catalytic performance. The potential of methanol to hydrogen depends on the catalyst with high selectivity for hydrogen at low temperatures. Therefore, the steam reforming of methane over the Sr-doped LaCeO_{3-δ} catalyst shows good promise for the development of an efficient, economical and clean hydrogen production system.

Author Contributions: Conceptualization, Q.S.; methodology, Z.C.; software, Z.S.; formal analysis, S.L.; writing—original draft preparation, G.C.; writing—review and editing, Q.S.; data curation, X.Z.; supervision, G.Y. All authors have read and agreed to the published version of the manuscript.

Funding: This work was supported by China Postdoctoral Science Foundation (No.2019M651094) and Science and Technology Innovation Foundation of Dalian (2021JJ11CG004).

Institutional Review Board Statement: Not applicable.

Informed Consent Statement: Not applicable.

Data Availability Statement: Not applicable.

Conflicts of Interest: The authors declare no conflict of interest.

References

1. Chiu, M.; Kuo, C.; Huang, C.; Yang, W. Preparation of CuS/PbS/ZnO Heterojunction Photocatalyst for Application in Hydrogen Production. *Catalysts* **2022**, *12*, 1677. [[CrossRef](#)]
2. Anandarajah, G.; McDowall, W.; Ekins, P. Decarbonising road transport with hydrogen and electricity: Long term global technology learning scenarios. *Int. J. Hydrog. Energy* **2013**, *38*, 3419–3432. [[CrossRef](#)]
3. Dutta, S. A review on production, storage of hydrogen and its utilization as an energy resource. *J. Ind. Eng. Chem.* **2014**, *20*, 1148–1156. [[CrossRef](#)]
4. Cheng, Z.; Zhou, W.; Lan, G.; Sun, X.; Wang, X.; Jiang, C.; Li, Y. High-performance Cu/ZnO/Al₂O₃ catalysts for methanol steam reforming with enhanced Cu-ZnO synergy effect via magnesium assisted strategy. *J. Energy Chem.* **2021**, *63*, 550–557. [[CrossRef](#)]
5. Aramouni, N.A.K.; Touma, J.G.; Tarboush, B.A.; Zeaiter, J.; Ahmad, M.N. Catalyst design for dry reforming of methane: Analysis review. *Renew. Sustain. Energy Rev.* **2018**, *82*, 2570–2585. [[CrossRef](#)]
6. Shen, Q.; Cai, Z.; Shao, Z.; Yang, G.; Li, S. Improved performance of bimetallic oxides CuO-Y₂O₃ synthesized by sol-gel for methanol steam reforming. *J. Am. Ceram. Soc.* **2022**, *105*, 6839–6850. [[CrossRef](#)]
7. Mosinska, M.; Stepińska, N.; Maniukiewicz, W.; Rogowski, J.; Mierczynska-Vasilev, A.; Vasilev, K.; Mierczynski, P. Hydrogen Production on Cu-Ni Catalysts via the Oxy-Steam Reforming of Methanol. *Catalysts* **2020**, *10*, 273. [[CrossRef](#)]
8. Nilsson, M.; Jozsa, P.; Pettersson, L.J. Evaluation of Pd-based catalysts and the influence of operating conditions for autothermal reforming of dimethyl ether. *Appl. Catal. B: Environ.* **2007**, *76*, 42–50. [[CrossRef](#)]
9. Vidal Vázquez, F.; Simell, P.; Pennanen, J.; Lehtonen, J. Reactor design and catalysts testing for hydrogen production by methanol steam reforming for fuel cells applications. *Int. J. Hydrog. Energy* **2016**, *41*, 924–935. [[CrossRef](#)]
10. Wu, G.; Li, S.; Zhang, C.; Wang, T.; Gong, J. Glycerol steam reforming over perovskite-derived nickel-based catalysts. *Appl. Catal. B: Environ.* **2014**, *144*, 277–285. [[CrossRef](#)]
11. Zhang, Y.; Guo, L.; Xu, Q.; Zhang, Q.; Li, J.; Ma, Q. Effect of Sr-Doping on the Photocatalytic Performance of LaNiO_{3-σ}. *Catalysts* **2022**, *12*, 1434. [[CrossRef](#)]
12. Morales, M.; Segarra, M. Steam reforming and oxidative steam reforming of ethanol over La_{0.6}Sr_{0.4}CoO_{3-δ} perovskite as catalyst precursor for hydrogen production. *Appl. Catal. A Gen.* **2015**, *502*, 305–311. [[CrossRef](#)]
13. Ma, F.; Ding, Z.; Chu, W.; Hao, S.; Qi, T. Preparation of LaXCoO₃ (X = Mg, Ca, Sr, Ce) catalysts and their performance for steam reforming of ethanol to hydrogen. *Chin. J. Catal.* **2014**, *35*, 1768–1774. [[CrossRef](#)]
14. Cui, Y.; Galvita, V.; Rihko-Struckmann, L.; Lorenz, H.; Sundmacher, K. Steam reforming of glycerol: The experimental activity of La_{1-x}Ce_xNiO₃ catalyst in comparison to the thermodynamic reaction equilibrium. *Appl. Catal. B: Environ.* **2009**, *90*, 29–37. [[CrossRef](#)]
15. Gómez-Cuaspad, J.A.; Perez, C.A.; Schmal, M. Nanostructured La_{0.8}Sr_{0.2}Fe_{0.8}Cr_{0.2}O₃ Perovskite for the Steam Methane Reforming. *Catal. Lett.* **2016**, *146*, 2504–2515. [[CrossRef](#)]
16. Natile, M.M.; Poletto, F.; Galenda, A.; Glisenti, A.; Montini, T.; Rogatis, L.D.; Fornasiero, P. La_{0.6}Sr_{0.4}Co_{1-y}Fe_yO_{3-δ} perovskites: Influence of the Co/Fe atomic ratio on properties and catalytic activity toward alcohol steam-reforming. *Chem. Mater.* **2008**, *20*, 2314–2327. [[CrossRef](#)]
17. Shao, Z.; Shen, Q.; Ding, H.; Jiang, Y.; Li, S.; Yang, G. Synthesis, characterization, and methanol steam reforming performance for hydrogen production on perovskite-type oxides SrCo_{1-x}Cu_xO_{3-δ}. *Ceram Int.* **2022**, *48*, 11836–11848. [[CrossRef](#)]
18. Shen, Q.; Shao, Z.; Cai, Z.; Yan, M.; Yang, G.; Li, S. Enhancement of hydrogen production performance of novel perovskite LaNi_{0.4}Al_{0.6}O_{3-δ} supported on MOF A520-derived λ-Al₂O₃. *Int. J. Energy Res.* **2022**, *46*, 15709–15721. [[CrossRef](#)]
19. Shen, Q.; Li, S.; Yang, G.; Yuan, J.; Huang, N. Development of microwave-assisted sol-gel rapid synthesis of nano-crystalline perovskites oxygen carrier material in oxyfuel combustion. *J. Ceram. Process. Res.* **2019**, *20*, 152–157. [[CrossRef](#)]
20. Mangu, S.; Soares, V.; Gupta, A.; Anantharaman, A.P. Synthesis, characterization and density Functional theory (DFT) study of LaCeO₃. *Mater. Today: Proc.* **2022**, *57*, 1892–1897. [[CrossRef](#)]
21. Jangam, A.; Das, S.; Pati, S.; Kawi, S. Catalytic reforming of tar model compound over La_{1-x}Sr_xCo_{0.5}Ti_{0.5}O_{3-δ} dual perovskite catalysts: Resistance to sulfide and chloride compounds. *Appl. Catal. A: Gen.* **2021**, *613*, 118013. [[CrossRef](#)]
22. Xu, X.; Shuai, K.; Xu, B. Review on Copper and Palladium Based Catalysts for Methanol Steam Reforming to Produce Hydrogen. *Catalysts* **2017**, *7*, 183. [[CrossRef](#)]
23. Luan, X.; Qi, L.; Zheng, Z.; Gao, Y.; Xue, Y.; Li, Y. Step by Step Induced Growth of Zinc-Metal Interface on Graphdiyne for Aqueous Zinc-Ion Batteries. *Angew. Chem. Int. Ed.* **2023**. [[CrossRef](#)]

24. Shen, Q.; Li, S.; Yang, G.; Sunden, B.; Yuan, J. Effect of A-/B-site Doping on Oxygen Non-Stoichiometry, Structure characteristics, and O₂ Releasing Behavior of La_{1-x}Ca_xCo_{1-y}Fe_yO_{3-δ} Perovskites. *Energies* **2019**, *12*, 410. [[CrossRef](#)]
25. Yang, P.; Li, N.; Teng, J.; Wu, J.; Ma, H. Influence of A-site cation in La_{0.7}M_{0.3}Ni_{0.7}Fe_{0.3}O₃ (M = Pr, Y, Sr, Zr, Ce) perovskite-type oxides on the catalytic performance. *Chem. Res. Appl.* **2018**, *30*, 1979–1985.
26. Shen, Q.; Dong, S.; Li, S.; Yang, G.; Pan, X. A Review on the Catalytic Decomposition of NO by Perovskite-Type Oxides. *Catalysts* **2021**, *11*, 622. [[CrossRef](#)]
27. Mukai, D.; Izutsu, Y.; Sekine, Y. Highly and stably dispersed Pt catalysts supported over La_{1-x}Sr_xAlO_{3-0.5x} perovskite for oxidative methane activation and their structures. *Appl. Catal. A Gen.* **2013**, *458*, 71–81. [[CrossRef](#)]
28. Da Silva Veras, T.; Mozer, T.S.; da Costa Rubim Messeder dos Santos, D.; da Silva César, A. Hydrogen: Trends, production and characterization of the main process worldwide. *Int. J. Hydrog. Energy* **2017**, *42*, 2018–2033. [[CrossRef](#)]
29. Yang, E.; Noh, Y.; Hong, G.; Moon, D. Combined steam and CO₂ reforming of methane over La_{1-x}Sr_xNiO₃ perovskite oxides. *Catal. Today* **2018**, *299*, 242–250. [[CrossRef](#)]
30. Shen, Q.; Zheng, Y.; Luo, C.; Ding, N.; Zheng, C.; Thern, M. Effect of A/B-site substitution on oxygen production performance of strontium cobalt based perovskites for CO₂ capture application. *RSC Adv.* **2015**, *5*, 39785–39790. [[CrossRef](#)]
31. Abdalla, A.M.; Hossain, S.; Nisfindy, O.B.; Azad, A.T.; Dawood, M.; Azad, A.K. Hydrogen production, storage, transportation and key challenges with applications: A review. *Energy Convers. Manag.* **2018**, *165*, 602–627. [[CrossRef](#)]
32. Shen, Q.; Jiang, Y.; Li, S.; Yang, G.; Zhang, H.; Zhang, Z.; Pan, X. Hydrogen production by ethanol steam reforming over Ni-doped LaNi_xCo_{1-x}O_{3-δ} perovskites prepared by EDTA-citric acid sol-gel method. *J. Sol-Gel Sci. Technol.* **2021**, *99*, 420–429. [[CrossRef](#)]
33. Ding, H.; Xu, Y.; Luo, C.; Wang, Q.; Li, S.; Cai, G.; Zhnag, L.; Zhang, Y.; Shen, Q. Oxygen desorption behavior of sol-gel derived perovskite-type oxides in a pressurized fixed bed reactor. *Chem Eng. J.* **2017**, *323*, 340–346. [[CrossRef](#)]

Disclaimer/Publisher's Note: The statements, opinions and data contained in all publications are solely those of the individual author(s) and contributor(s) and not of MDPI and/or the editor(s). MDPI and/or the editor(s) disclaim responsibility for any injury to people or property resulting from any ideas, methods, instructions or products referred to in the content.